Eur. Phys. J. E (2013) **36**: 22
DOI 10.1140/epje/i2013-13022-3

THE EUROPEAN PHYSICAL JOURNAL E

Regular Article

Wrinkling in the deflation of elastic bubbles

Elodie Aumaitre[1], Sebastian Knoche[2], Pietro Cicuta[1,a], and Dominic Vella[3,4]

[1] Cavendish Laboratory, University of Cambridge, JJ Thomson Avenue, CB3 0HE Cambridge, UK
[2] Faculty of Physics, Technische Universität Dortmund, 44221 Dortmund, Germany
[3] OCCAM, Mathematical Institute, 24-29 St Giles', Oxford, OX1 3LB, UK
[4] Department of Applied Mathematics and Theoretical Physics, University of Cambridge, Wilberforce Road, Cambridge CB3 0WA, UK

Received 14 July 2012 and Received in final form 11 December 2012
Published online: 18 March 2013 –

Abstract. The protein hydrophobin HFBII self-assembles into very elastic films at the surface of water; these films wrinkle readily upon compression. We demonstrate and study this wrinkling instability in the context of non-planar interfaces by forming HFBII layers at the surface of bubbles whose interfaces are then compressed by deflation of the bubble. By varying the initial concentration of the hydrophobin solutions, we are able to show that buckling occurs at a critical packing fraction of protein molecules on the surface. Independent experiments show that at this packing fraction the interface has a finite positive surface tension, and not zero surface tension as is usually assumed at buckling. We attribute this non-zero wrinkling tension to the finite elasticity of these interfaces. We develop a simple geometrical model for the evolution of the wrinkle length with further deflation and show that wrinkles grow rapidly near the needle (used for deflation) towards the mid-plane of the bubble. This geometrical model yields predictions for the length of wrinkles in good agreement with experiments independently of the rheological properties of the adsorbed layer.

1 Introduction

From the formation of finger prints [1] to geological structures [2], the buckling of thin sheets in various situations can be explained by the onset of an elastic instability in which an in-plane compression leads to an out-of-plane deformation. The theory of elasticity of a beam or a plate [3] can be used to predict the wavelength and amplitude of the wrinkles by balancing the bending and stretching energies [4, 5]. Conversely, buckling instabilities have frequently been used to infer properties of materials, such as Young's modulus and thickness, based on measurements of the wrinkling pattern [6, 7].

Wrinkling is also observed in materials with more complicated rheologies than simple Hookean solids. For example, wrinkling has been observed in surfactant and protein monolayers [8,9] as well as in "particle rafts" [10,11]. While these systems have been well studied, theoretical models are often based on the assumption that buckling occurs when the interfacial tension vanishes (so that deformation out of the plane costs little or no surface energy). This hypothesis has been verified experimentally for films with no significant elastic shear modulus, such as lung surfactants [8]. However, for films with notable elastic shear modulus the stress within the film need not be isotropic and homogeneous. Indeed, the literature provides many examples of layers buckling before the apparent interfacial tension reaches zero. For example, interfaces coated with spherical [12] and ellipsoidal [13] colloidal particles buckle upon compression whilst the measured interfacial tension is still a significant fraction of its value before coating. This discrepancy is most likely explained by the localized nature of the wrinkling pattern: the interfacial tension is usually measured away from the wrinkled region and so does not preclude the possibility that the stress really does collapse in the wrinkled region.

Although commonly observed, the buckling of layers with finite shear modulus has yet to be fully understood from a theoretical point of view. Various models based on the mechanics of thin elastic sheets have been proposed to explain the observed wavelength of wrinkles [10, 14]. It is also observed that folds may develop from wrinkles in such systems [8, 15]; an observation that sparked considerable theoretical work on the nature of the transition from wrinkles to folds [16, 17]. However, such elastic-based theories are currently unable to explain the various empirical relationships between the geometry of the experimental apparatus and the surface tension that is measured at the onset of buckling, which have been reported recently [11,18]. The question then arises: are these features due to inho-

[a] e-mail: pc245@cam.ac.uk

mogeneous packing of the molecules at the interface or rather a combination of elasticity and geometry?

The observation that the onset of wrinkling has a vital geometrical aspect makes it surprising that most studies of the buckling and collapse of interfacial monolayers focus largely on compression in planar geometries such as a Langmuir trough. Recently, Stanimirova *et al.* [19] have observed wrinkles on a pendant droplet covered by the surfactant Saponin, which has the potential to develop highly elastic monolayers. Here, we develop a controlled setup to investigate the wrinkling of hydrophobin HFBII films on the surface of a bubble where the compression of the interface is achieved by deflation of the bubble. Our use of the protein hydrophobin HFBII is motivated by recent interest in its ability to self-assemble into highly elastic films. This high level of elasticity is believed to explain HFBII's capacity to stabilize foams on long timescales [20,21] which in turn makes it of interest in a range of food and medical applications. We focus on studying the wrinkling of hydrophobin films in this geometry since it is both one of practical interest and because it removes some of the limitations of studying wrinkling in planar Langmuir troughs, such as friction with side walls [18]. We show that buckling appears to occur when the hydrophobin layer reaches a critical surface concentration but also demonstrate that some features of the problem, such as the rapid rate at which wrinkles grow with further compression, can be understood using purely geometrical ideas.

2 Experiment

Class II hydrophobin (HFBII) from *Trichoderma reesei* was a gift from Unilever Global Development Centre and was obtained from VTT Biotechnology (Espoo, Finland). Details of the preparation are described elsewhere [22,23]. A drop tensiometer (First Ten Angstroms, UK) comprising of a precise microstage and a camera was used for the buckling experiment. A bubble was formed at the tip of a J-needle dipped into a cuvette filled with a hydrophobin solution, left to equilibrate for 20 minutes (to reach the equilibrium surface tension of the surrounding solution), and then deflated by sucking the air back into the syringe gently, see fig. 1.

The equilibrium surface tension of hydrophobin solutions of varying concentrations, was characterized by Wilhelmy plate tensiometry at a planar interface (process tensiometer K12, Kruss GmbH, Hamburg). These data then allow us, given a value of the surface tension of a solution, to infer the area per molecule, by comparison to surface compression isotherms with a known amount spread.

Prior to compression, the surface area of each bubble was measured (from images) and the number of molecules on the surface estimated from the bubble surface area and the hydrophobin molecular area. It should be emphasized here that the measurements of surface pressure returned by a Wilhelmy plate in a rigid layer might not correspond simply to the pure surface pressure [18]. However, this technique can still be useful to provide an idea of the surface area per molecule; other techniques, such as surface quasi-elastic light scattering can be used to measure compression isotherms [18,24] and yield similar values for the molecular area.

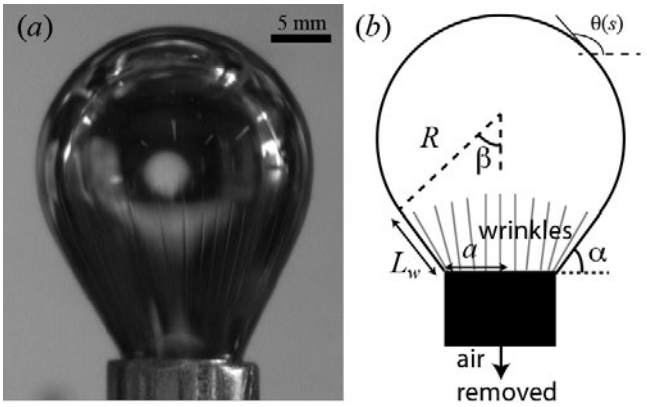

Fig. 1. Wrinkles form in hydrophobin-coated bubbles, under deflation. (a) Experimental image of a wrinkled bubble in hydrophobin solution. The bubble is initially allowed to equilibrate with the bulk solution before it is deflated causing the wrinkling seen here. (b) Schematic diagram illustrating the model parameters used here, namely the radius of the needle to which the bubble is attached, a, the typical radius of curvature of the bubble, R, and the length of the wrinkled portion L_w.

The volume and surface area at which the bubble first wrinkles can be recorded, as well as the length of the wrinkles. J-needles with outer diameters of 0.75 mm and 1.25 mm were made by bending blunt stainless steel needles with round pliers. The experiment was repeated varying the initial volume of the bubble (typically between 2 and 10 μL) and the surface tension of the bulk hydrophobin solution.

3 Results

Our measurement of the surface pressure isotherm for hydrophobin is shown in fig. 2(a) together with the inferred values of the initial molecular area for the bubbles in our experiments before deflation, and at the onset of wrinkling. Note that there is a region of concentration that can be reliably measured by both Wilhelmy plate and light scattering (SQELS). SQELS is described in previous work [24]. At lower pressures, the Wilhelmy plate measures a lower pressure than SQELS, since SQELS is more sensitive to localised, tenuous structures that form in dilute conditions, as described previously [24]. At higher pressures, the elastic stress in the layer builds up and affects the different experimental probes in different ways. These measurements, on "flat" interfaces, give us a reference for comparing to the compression of monolayers formed on bubbles.

Whilst the molecular scale structure of hydrophobin monolayers has not yet been fully established, the qualitative picture we have in mind is of hydrophobin as a core-shell unit, with a hard core and a semi-soft shell. This type of object will form a close-packing of the semi-soft shells,

which is manifested in the surface pressure isotherms as a drastic increase in pressure from near zero. Shear elasticity begins to build up from that point. There is then a second concentration, where the hard cores are packed, and the layer cannot compress further in-plane, and so buckles.

Figure 2(b) shows that the bubble surface area at the onset of wrinkling is directly proportional to the number of molecules adsorbed at the bubble interface before its deflation. Each marker corresponds to an independent deflation experiment; the concentration of the hydrophobin solution and the bubble volume were varied between experiments. We can see that all of these data collapse on to a single straight line. This suggests that the wrinkles arise when the molecules have reached a given packing, and this occurs at a molecular area of around 410 Å^2, as seen in fig. 2(a). From the observed molecular area at the onset of wrinkling and the surface pressure isotherm, we estimate that the apparent surface tension at wrinkling ($\gamma_{\rm wrink} = \gamma_C - \Pi \simeq 72.8 - 30 \simeq 42.8$ mN/m) is non-zero. This value is consistent with observations by Kisko *et al.* [25] on hydrophobin HFBII films, who imaged the collapse of the layer by Brewster Angle Microscopy at a surface pressure ≥ 30 mN/m.

The observation that wrinkling occurs at a well-defined molecular packing, and that this packing corresponds to an apparent positive surface tension, suggests that the packing of molecules on the surface is likely to be homogeneous. Nevertheless since wrinkles are observed, the state of stress in the bubble's surface is necessarily anisotropic and inhomogeneous. We also note that at this point in the surface pressure isotherm the rheology of the interface is changing rapidly with small variations in the compression. We emphasise that the molecular packing at wrinkling appears to be homogeneous and independent of the initial size of the bubble suggesting that it is a combination of elastic and geometric effects only that give rise to wrinkling (*i.e.* it is not an accumulation of hydrophobin molecules in one region of the bubble decreasing the surface tension there to zero).

Once wrinkles have appeared near the needle, their length grows dramatically as the bubble is deflated further. This is illustrated in fig. 3, which shows the wrinkle length as a function of bubble volume for a range of initial bubble volumes and bulk solution concentrations. We present a minimal model aimed at explaining this observation; this model highlights the role that the system geometry plays in the development of the wrinkling pattern without the need for detailed rheological models of the interface.

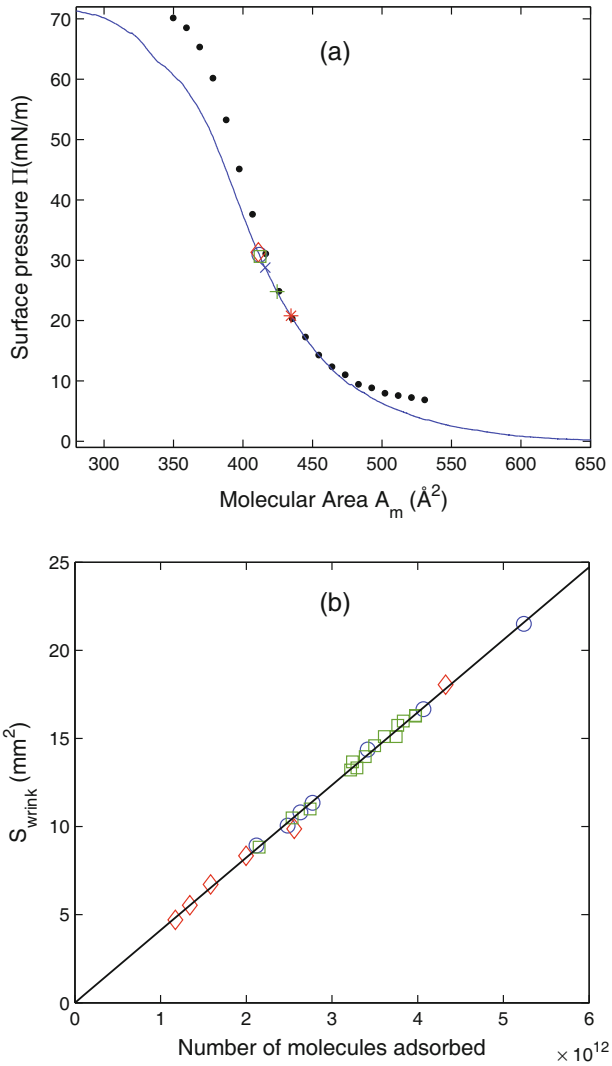

Fig. 2. Wrinkling takes place at a well-defined area per molecule, and the tension at this molecular area is finite. (a) For each experiment, the initial surface pressures before compression (∗, +, × for hydrophobin solutions with surface tensions of 52 mN/m, 48 mN/m and 44 mN/m, respectively) are reported on an isotherm of compression (solid line). Together with the initial surface area of the bubble, this allows us to estimate the number of molecules adsorbed at the bubble interface. The solid dots mark the pressure measured by surface light scattering from thermal fluctuations [24], which is is agreement with the Wilhelmy plate data over the range of interest. (b) The surface area of the bubble when the first wrinkles appear is proportional to the number of hydrophobin molecules adsorbed. Each marker represents a single compression experiment. All the data collapse onto a single straight line, indicating that buckling occurs when the hydrophobin molecules have reached a given packing. The three sets of data (◇, □,○) correspond to the onset of wrinkling in hydrophobin solutions with surface tensions of 52 mN/m, 48 mN/m and 44 mN/m, respectively, in both panels. Given the "compression factor" to buckling, it is possible for each bulk concentration to infer the corresponding area per molecule at buckling: These are marked by open symbols in panel (a), and coincide to within experimental accuracy. Note that the corresponding pressure is well below 72 mN/m.

4 A geometrical model

Previous studies have shown that the rheology of interfacial layers is complicated: the effective elastic moduli depend on the packing fraction of the molecules at the interface [26]. Here, therefore, we develop a model that bypasses the mechanical properties of the interface and focuses solely on the geometrical aspects of wrinkling.

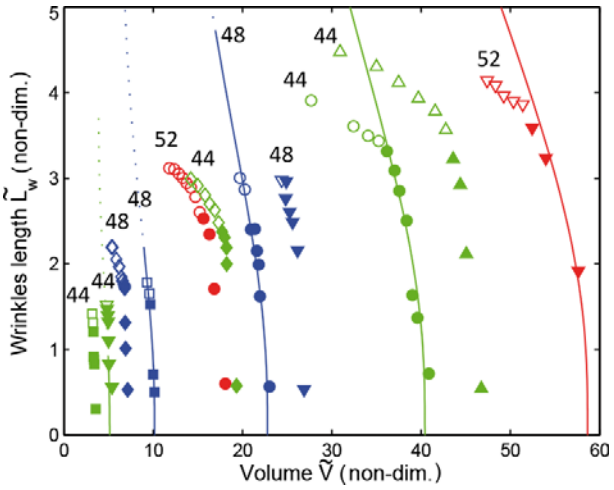

Fig. 3. The experimental wrinkle length can be described theoretically by a simple geometrical model with no fitting parameter. As the bubble volume is reduced, wrinkles grow from the needle. The data here are the dimensionless wrinkle length, as a function of bubble volume. Lengths are non-dimensionalized by the radius of the needle, a, and volumes by a^3. Markers represent experimental data, at three different equilibrium values of the hydrophobin solution surface tensions (values as marked, in mN/m). Lines show the theoretical predictions from the minimal geometrical model presented in the main text, in excellent agreement for wrinkles up to the mid-plane of the bubbles. The growth of the wrinkles beyond the mid-plane of the bubble is shown by open markers (experiments) and dashed curves (theory): In this case the wrinkled region is noticeably curved in experiments, while the model maintains the assumption of a straight wrinkled region.

Our model is based on the observation that the wrinkled bubble may be approximately divided into a wrinkled part, in which the interface makes a constant angle α with the horizontal, and an unwrinkled, spherical cap. We note that with this assumption, elementary geometry ensures that $\alpha = \beta$, with α and β defined in fig. 1. The advantage of these simplifications is two-fold: firstly this model is analytically tractable, secondly we neglect the details of the stress state within the bubble, which depends on both the detailed rheology of the interface as well as the history of bubble deformations from an initial condition [27]. To close the model, we assume that the surface area of the bubble is fixed at its value at the onset of wrinkling, $S = S_{\text{wrink}}$; this corresponds to assuming that the molecules are already at maximum packing and cannot pack further.

The connection between the wrinkled and unwrinkled parts occurs at an unknown arclength $s = L_w$. The position of the boundary of the wrinkled region, L_w must be determined as part of the solution of the problem. Indeed, the position of the wrinkle extent has recently been a focus of considerable theoretical and experimental effort in related systems [7, 28–30]. We therefore focus on understanding the evolution of the wrinkle length as the volume of the bubble is decreased further beyond the onset of wrinkling.

The surface area of the bubble is the sum of that of the section of a cone (the wrinkled region) and a spherical cap of radius R (the unwrinkled region), which may be expressed as

$$\tilde{S} = \frac{S}{a^2} = \frac{\pi}{\cos\alpha}\left[\frac{R^2}{a^2}(1+\cos\alpha)^2 - 1\right], \qquad (1)$$

while the volume is

$$\tilde{V} = \frac{V}{a^3} = \frac{\pi}{3}\left[\frac{R^3}{a^3}\frac{(1+\cos\alpha)^2}{\cos\alpha} - \tan\alpha\right]. \qquad (2)$$

Here we are using the radius of the needle, a, to non-dimensionalize. (We use this length scale because neglecting the stresses within the membrane removes both surface tension and gravity from the problem, and hence the capillary length is no longer a relevant length scale; the only remaining length scale is then a.) $\tilde{S}$ and $\tilde{V}$ are thus the dimensionless surface area and volume of the bubble, respectively. Geometry may also be used to show that the dimensionless length of the wrinkles is given by

$$\tilde{L}_w = \frac{L_w}{a} = \frac{R}{a}\tan\alpha - \sec\alpha. \qquad (3)$$

For a given initial surface area at the wrinkling point $\tilde{S} = \tilde{S}_w$, we may use the angle α to parametrize the bubble shapes with this $\tilde{S}$. To do this, we calculate the bubble radius $R(\tilde{S}_w;\alpha)$ from (1) and use this value in (2) and (3) to give the corresponding bubble volume and wrinkle length. In this way, it is possible to plot the wrinkle length as a function of bubble volume for different initial surface areas. Such a plot is shown in fig. 3 for a variety of different values of $\tilde{S}_w$. We note that the agreement between theoretical predictions for the length of the wrinkles and experimental observations is extremely good; we emphasize especially that there are no fitting parameters in this model.

The most striking feature of the theoretical and experimental curves in fig. 3 is that the curves are normal to the x-axis at the point where they intersect it: the wrinkle length grows continuously (cf. a second-order phase transition) rather than discontinuously. This result may be demonstrated analytically by showing that the derivative $V'(\alpha_0) = 0$, where α_0 is such that $L_w(\alpha_0) = 0$, which in turn requires that $R(\alpha_0)\sin\alpha_0 = a$.

5 Conclusion

We have studied the deflation-induced buckling of bubbles coated by hydrophobin. This is novel both in the sense that wrinkled bubbles may be of interest in applications and also because it may enable the future study of the rheology of such interfaces in more realistic, curved geometries than the use of a Langmuir trough currently allows. This latter feature is particularly important since numerous studies have shown that the use of a Langmuir trough and Wilhelmy plate introduce geometrical complications that may invalidate results for practically relevant scenarios [11, 18].

Our study has shown that the wrinkling instability first occurs when the molecules reach a critical packing fraction. The presence of elastic effects within the interface means that the effective surface tension of the interface does not vanish at this packing fraction. Furthermore, the geometrical nature of the wrinkling instability was highlighted by a simple geometrical model using a minimal set of physically based assumptions that was able to predict the evolution of the length of wrinkles post buckling.

We intend to study this wrinkling in more detail in the future, both with this system and with similar layers that have a better characterized rheology. Of special interest here is the fact that the resulting shells have negligible bending stiffness, as measured by the "bendability" [30]

$$\epsilon^{-1} = \frac{p^2 R^4}{EhB} \gg 1, \tag{4}$$

where E denotes the Young modulus, B the bending stiffness, h the shell thickness and R the typical radius. We therefore expect the wrinkling of such shells upon deflation to be in the "far-from-threshold" regime [30,31].

EPSRC and Unilever plc. have funded this project through a CASE award. This publication is based on work supported in part by Grant No. KUK-C1-013-04, made by King Abdullah University of Science and Technology (KAUST) and in part by an Oppenheimer Early Career Research Fellowship (D.V.).

References

1. M. Kucken, A.C. Newell, Europhys. Lett. **68**, 141 (2004).
2. P.J. Hudleston, L. Lan, J. Struct. Geol. **15**, 253 (1993).
3. L. Landau, E. Lifshitz, A. Kosevich, L. Pitaevskii, J. Sykes, W. Reid, *Theory of Elasticity* (Butterworth-Heinemann, 1986).
4. S. Milner, J. Joanny, P. Pincus, Europhys. Lett. **9**, 495 (1989).
5. E. Cerda, L. Mahadevan, Phys. Rev. Lett. **90**, 074302 (2003).
6. C.M. Stafford, C. Harrison, K.L. Beers, A. Karim, E.J. Amis, M.R. VanLandingham, H.C. Kim, W. Volksen, R.D. Miller, E.E. Simonyi, Nat. Mater. **3**, 545 (2004).
7. J. Huang, M. Juszkiewicz, W.H. de Jeu, E. Cerda, T. Emrick, N. Menon, T.P. Russell, Science **317**, 650 (2007).
8. L. Pocivavsek, S.L. Frey, K. Krishan, K. Gavrilov, P. Ruchala, A.J. Waring, F.J. Walther, M. Dennin, T.A. Witten, K.Y.C. Lee, Soft Matter **4**, 2019 (2008).
9. P. Erni, H.A. Jerri, K. Wong, A. Parker, Soft Matter **8**, 6958 (2012).
10. D. Vella, P. Aussillous, L. Mahadevan, Europhys. Lett. **68**, 212 (2004).
11. P. Cicuta, D. Vella, Phys. Rev. Lett. **102**, 138302 (2009).
12. D. Zang, A. Stocco, D. Langevin, B. Wei, B.P. Binks, Phys. Chem. Chem. Phys. **11**, 9522 (2009).
13. M.G. Basavaraj, G.G. Fuller, J. Fransaer, J. Vermant, Langmuir **22**, 6605 (2006).
14. Q. Zhang, T.A. Witten, Phys. Rev. E **76**, 041608 (2007).
15. L. Pocivavsek, B. Leahy, N. Holten-Andersen, B. Lin, K.Y.C. Lee, E. Cerda, Soft Matter **5**, 1963 (2009).
16. B. Audoly, Phys. Rev. E **84**, 011605 (2011).
17. H. Diamant, T.A. Witten, Phys. Rev. Lett. **107**, 164302 (2011).
18. E. Aumaitre, D. Vella, P. Cicuta, Soft Matter **7**, 2530 (2011).
19. R. Stanimirova, K. Marinova, S. Tcholakova, N.D. Denkov, S. Stoyanov, E. Pelan, Langmuir **27**, 12486 (2011).
20. A.R. Cox, F. Cagnol, A.B. Russell, M.J. Izzard, Langmuir **23**, 7995 (2007).
21. N.A. Alexandrov, K.G. Marinova, T.D. Gurkov, K.D. Danov, P.A. Kralchevsky, S.D. Stoyanov, T.B. Blijdenstein, L.N. Arnaudov, E.G. Pelan, A. Lips, J. Colloid Interface Sci. **376**, 296 (2012).
22. M.J. Bailey, S. Askolin, N. Horhammer, M. Tenkanen, M. Linder, M. Penttila, T. Nakari-Setala, Appl. Microbiol. Biotech. **58**, 721 (2002).
23. M. Linder, K. Selber, T. Nakari-Setala, M. Qiao, M.R. Kula, M. Penttila, Biomacromolecules **2**, 511 (2001).
24. E. Aumaitre, S. Wongsuwarn, D. Rossetti, N.D. Hedges, A.R. Cox, D. Vella, P. Cicuta, Soft Matter **8**, 1175 (2012).
25. K. Kisko, G.R. Szilvay, E. Vuorimaa, H. Lemmetyinen, M.B. Linder, M. Torkkeli, R. Serimaa, Langmuir **25**, 1612 (2009).
26. G.G. Fuller, J. Vermant, Annu. Rev. Chem. Biomol. Engin. **3**, 519 (2012).
27. S. Knoche, Master's thesis, Technische Universitat Dortmund (2011).
28. D. Vella, M. Adda-Bedia, E. Cerda, Soft Matter **6**, 5778 (2010).
29. D. Vella, A. Ajdari, A. Vaziri, A. Boudaoud, Phys. Rev. Lett. **107**, 174301 (2011).
30. B. Davidovitch, R.D. Schroll, D. Vella, M. Adda-Bedia, E. Cerda, Proc. Natl. Acad. Sci. U.S.A. **108**, 18227 (2011).
31. M. Stein, J.M. Hedgepeth, Tech. Rep. NASA (1961).